Erzincan Üniversitesi
Fen Bilimleri Enstitüsü Dergisi
2022, 15(2), 592-608
ISSN: 1307-9085, e-ISSN: 2149-4584
Araştırma Makalesi

Erzincan University
Journal of Science and Technology
2022, 15(2), 592-608
DOI: 10.18185/erzifbed.1123429
Research Article

# Analysis of the Molecular Structure of N'-((2-hydroxynaphthalen-1-yl)methylene)isobutyrohydrazide

Çiğdem YÜKSEKTEPE ATAOL*

Cankiri Karatekin University, Faculty of Science, Department of Physics, 18100, Çankırı, Turkey
ORCID number 0000-0001-6098-0328

Geliş / Received: 30/05/2022, Kabul / Accepted: 11/08/2022

**Abstract**

In this study, the molecular structure of N'-((2-hydroxynaphthalin-1-yl)methylene)isobutyrohydrazide compound with the closed formula $C_{15}H_{16}N_2O_2$ was investigated by using the Density Functional Theory (DFT) hybrid basis functions B3LYP and 6-311+G(d, p) basis set. The molecular structure of the compound $C_{15}H_{16}N_2O_2$ was first optimized in gas, chloroform, ethanol and water environments. Then, molecular electrostatic potential (MEP) map was obtained by using optimized molecular structures, molecular orbital energy levels and energy values were investigated in different solvent environments. Chemical reactivity parameters were derived from the molecular orbital energy values obtained for different environments. By using the Time Dependent Density Functional Theory (TD-DFT), the UV spectra of the compound in the excited state were calculated for different environments and the percentage contributions from atomic orbitals to molecular orbitals were calculated. Finally, the interaction between some heavy metals such as Sn, Hg, Cd and Zn and the $C_{15}H_{16}N_2O_2$ compound was investigated by using the (ΔN) charge transfer and (ΔE) energy lowering values of the molecular structure.

**Keywords**: density functional theory, chemical reactivity, ligand-metal interaction

## N'-((2-hidroksinaftalin-1-yl)metilen)izobütirohidrazidin Moleküler Yapısının Analizi

**Öz**

Bu çalışmada kapalı formülü $C_{15}H_{16}N_2O_2$ olan N'-((2-hidroksinaftalin-1-yl)metilen)izobütirohidrazid bileşiğinin moleküler yapısı Yoğunluk Fonksiyonel Teorisi (YFT) hibrid baz fonksiyonlarından B3LYP ve 6-311+G(d, p) baz seti kullanılarak araştırılmıştır. $C_{15}H_{16}N_2O_2$ bileşiğinin moleküler yapısı, ilk olarak gaz, kloroform, etanol ve su ortamlarında optimize edilmiştir. Daha sonra optimize edilen moleküler yapılar kullanılarak moleküler elektrostatik potansiyel (MEP) haritası elde edilmiş, farklı çözücü ortamlarında moleküler orbital enerji seviyeleri ve enerji değerleri araştırılmıştır. Farklı ortamlar için elde edilen moleküler orbital enerji değerlerinden kimyasal reaktivite parametreleri türetilmiştir. Zamana Bağlı Yoğunluk Fonksiyonel Teorisi (ZB-YFT) kullanılarak farklı ortamlar için bileşiğin uyarılmış durumda UV spektrumları hesaplatılmış ve moleküler orbitallere atomik orbitallerin yüzde katkıları belirlenmiştir. Son olarak, moleküler yapının (ΔN) yük transfer ve (ΔE) enerji düşürme değerleri kullanılarak Sn, Hg, Cd ve Zn gibi bazı ağır metaller ile $C_{15}H_{16}N_2O_2$ bileşiği arasındaki etkileşim araştırılmıştır.

**Anahtar Kelimeler:** yoğunluk fonksiyonel teorisi, kimyasal reaktivite, ligant-metal etkileşimi

***CorrespondingAuthor: yuksektepe.c@karatekin.edu.tr**

## 1. Introduction

Hydrazones are characterized by the presence of the structural motif –CH = N–NH–C = O. Additional donor atoms such as N, O, and S in a suitable position for chelation make them more flexible and versatile. Therefore, hydrazones are good polydentate chelating agents that can form a variety of complexes with various metals and are often used as ligands in coordination chemistry [1].

Interest in metal complexes of Schiff bases (hydrazone) for the last 30 years increased, showing physiological activity, anti-tumor and anti-microbial activity and also they have gained a lot of importance due to the fact that they have and are used in pharmacy. However, Schiff bases are undesirable small amounts found in mineral oils. It is also used in the removal of elements, paint, rubber, pharmaceutical industry and agricultural purposes. Also in dyestuff and polymer technology, medicine, rocket fuel preparation, explanation of biological events and many other areas, compounds are widely used and new syntheses are needed work continues intensively [2].

Hydrazone compounds with potential biological activity and its metal complexes have been widely studied [3]. During recent years, many hydrazone compounds and their complexes have displayed novel structures and extensive applications in luminescent probes, antibacterial and antitumor agents, fluorescence markers, optical materials, and anticonvulsant agent [4]. In the past ten years, it has done some work in the synthesis, structural characterization, and properties of hydrazone compounds, which show novel structures and luminescent properties [5].

Naphthols have recently attracted much interest due to their large nonlinear optical properties (NLOP). This fact raised technological importance in various photonic technologies such as optical switching, optical communications, computing, wave guiding, compact 3D data storage and micro fabrication, chemical and biological sensing, optical power limiting, bioimaging, signal and data processing, and many other current items in materials science [6].

In this study, some important properties of the molecular structure of the $C_{15}H_{16}N_2O_2$ compound, which consists of functional groups such as hydrazone and naphthol, were investigated using DFT, one of the computational chemistry methods. The molecular structure was optimized in different solvent environments and the bond parameters were compared with the experimental parameters in the literature [2]. By calculating the total energy of the molecular structure, the most stable structure was obtained. Contributions to molecular orbital energy levels have been investigated. Ligand-metal interactions were investigated using the chemical reactivity parameters.

## 2. Material and Methods

Gaussian 09 program [7] was used to investigate the molecular structure of the $C_{15}H_{16}N_2O_2$ compound. The crystal structure of the $C_{15}H_{16}N_2O_2$ compound was previously elucidated in the literature, and the atomic coordinates (x, y, z) of the molecular structure were taken from the literature to save time in theoretical calculations. Density Functional Theory (DFT) was used

in the theoretical calculations. DFT is a quantum mechanics-based computational chemistry method developed with the Hohenberg-Kohn and Khon-Sham approximations. In addition, in this method, the Born-Oppenheimer approximation is made to calculate the Hamiltonian expression of a multi-electron system. To calculate the exchange and correlation energy in the energy eigenvalue of a multi-electron system, the [8] basis function, one of the hybrid functions, was used in the calculations. In these calculations, the diffuse-polarized 6-311+G(d, p) was chosen as the basis set.

## 3. Results and Discussion

### 3.1. The optimization of the molecular structure

The molecular structure of the $C_{15}H_{16}N_2O_2$ compound consisting of naphthol, hydrazone and isobutyric acid groups was optimized in the ground state and the B3LYP/6-311+G(d, p) basis set in both gas and solvent environments with different dielectric constant and polarity. As solvent media, chloroform, ethanol, and water media were chosen. This organic solvents have different dielectric constants and dipole moments; chloroform $\varepsilon = 4.81$, $\mu = 1.15$ D; ethanol $\varepsilon = 24.5$, $\mu = 1.69$ D; and water $\varepsilon = 80.1$, $\mu = 1.82$ D. The greater the dielectric constant influences the polarity (in this study; water = high, gas phase = low). Another effect is the dipole moment. The optimized molecular structure is given in Figure 3.1. Some selected bond parameters of the optimized molecular structure were compared with the experimental bond parameters in the literature and the bond parameters are given in Table 3.1. As can be seen from Table 3.1, there is not much difference between the calculated bond parameters and the experimental results. The best measure of how well experimental data fit a linear curve is regression. Regression analysis was performed to investigate the compatibility between the calculated bond parameters of the optimized molecular structure and its experimental parameters, and the results are given in Figures 3.2a and 3.2b. As can be seen from Figure 3.2 and Table 3.1, it can be said that the bond length and bond angle values obtained from solvent media are more compatible with the experimental results compared to the gas phase. In Figure 3.3, the overlapping of the molecular structure with the optimized structures obtained from gas and different solvent environments by the B3LYP/6-311+G(d, p) method and the experimentally obtained molecular structure is seen.

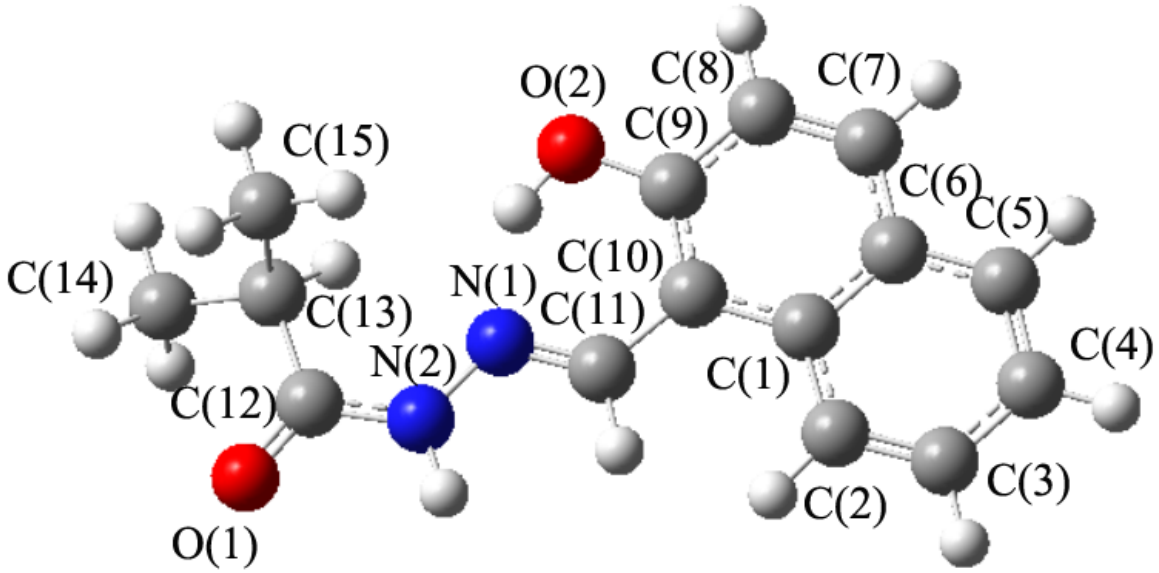


**Figure 3.1** The optimized molecular structure of the compound $C_{15}H_{16}N_2O_2$ in the water media by B3LYP/6-311+G(d, p)

**Table 3.1** The calculated and the experimental selected geometrical bond parameters of the compound $C_{15}H_{16}N_2O_2$

| | **X-ray [2]** | **B3LYP 6–311+G (d, p)** | **B3LYP 6–311+G (d, p) Ethanol** | **B3LYP 6–311+G (d, p) Chloroform** | **B3LYP 6–311+G (d, p) Water** |
|---|---|---|---|---|---|
| **Bond lengths (Å)** | | | | | |
| C(9)–O(2) | 1.355(3) | 1.345 | 1.351 | 1.349 | 1.351 |
| C(10)–C(11) | 1.451(4) | 1.451 | 1.452 | 1.452 | 1.452 |
| C(11)–N(1) | 1.287(4) | 1.293 | 1.294 | 1.293 | 1.294 |
| N(1)–N(2) | 1.382(3) | 1.361 | 1.365 | 1.364 | 1.365 |
| N(2)–C(12) | 1.350(4) | 1.386 | 1.370 | 1.374 | 1.369 |
| C(12)–O(1) | 1.238(3) | 1.218 | 1.230 | 1.227 | 1.231 |
| C(12)–C(13) | 1.501(4) | 1.524 | 1.524 | 1.523 | 1.523 |
| C(13)–C(14) | 1.527(4) | 1.532 | 1.532 | 1.532 | 1.532 |
| C(13)–C(15) | 1.519(5) | 1.543 | 1.544 | 1.543 | 1.544 |
| **$R^2$** | | 0.97193 | 0.98527 | 0.98319 | 0.98587 |
| **Bond angles (°)** | | | | | |

| | | | | | |
|---|---|---|---|---|---|
| O(2)–C(9)–C(10) | 122.9(3) | 122.93 | 122.50 | 122.63 | 122.49 |
| C(9)–C(10)–C(11) | 120.8(2) | 120.42 | 120.63 | 120.57 | 120.66 |
| C(10)–C(11)–N(1) | 121.8(3) | 122.77 | 122.15 | 122.35 | 122.07 |
| C(11)–N(1)–N(2) | 114.6(2) | 117.95 | 117.28 | 117.50 | 117.20 |
| N(1)–N(2)–C(12) | 122.4(3) | 125.05 | 124.17 | 124.41 | 124.13 |
| N(2)–C(12)–O(1) | 117.8(3) | 118.28 | 118.64 | 118.54 | 118.67 |
| N(2)–C(12)–C(13) | 120.1(3) | 117.70 | 118.12 | 118.00 | 118.16 |
| O(1)–C(12)–C(13) | 122.0(3) | 124.00 | 123.23 | 123.44 | 123.16 |
| C(12)–C(13)–C(14) | 109.8(3) | 110.31 | 110.85 | 110.70 | 110.90 |
| C(12)–C(13)–C(15) | 108.5(3) | 109.15 | 109.31 | 109.23 | 109.25 |
| **$R^2$** | | 0.90074 | 0.93543 | 0.92599 | 0.9384 |
| **Torsion angles (°)** | | | | | |
| O(2)–C(9)–C(10)−C(11) | 4.6(4) | -0.44 | -0.57 | -0.55 | -0.62 |
| C(9)–C(10)–C(11)−N(1) | -5.2(4) | 1.53 | 1.96 | 1.88 | 1.93 |
| C(10)–C(11)–N(1)−N(2) | 177.0(2) | -179.59 | -179.31 | -179.37 | -179.31 |
| C(11)–N(1)–N(2)−C(12) | -176.3(3) | -179.50 | -179.63 | -179.54 | -179.70 |
| N(1)–N(2)–C(12)−O(1) | 176.9(3) | -179.63 | -179.26 | -179.29 | -179.18 |
| N(1)–N(2)–C(12)−C(13) | -5.0(4) | -1.10 | -0.67 | -0.71 | -0.65 |
| N(2)–C(12)–C(13)−C(14) | 148.5(3) | 153.29 | 154.61 | 153.86 | 153.78 |
| N(2)–C(12)–C(13)−C(15) | -89.1(4) | -83.69 | -82.21 | -82.99 | -82.98 |
| O(1)–C(12)–C(13)−C(14) | -33.5(4) | -28.28 | -26.86 | -27.63 | -27.76 |
| O(1)–C(12)–C(13)−C(15) | 88.9(4) | 94.75 | 96.32 | 95.52 | 95.48 |

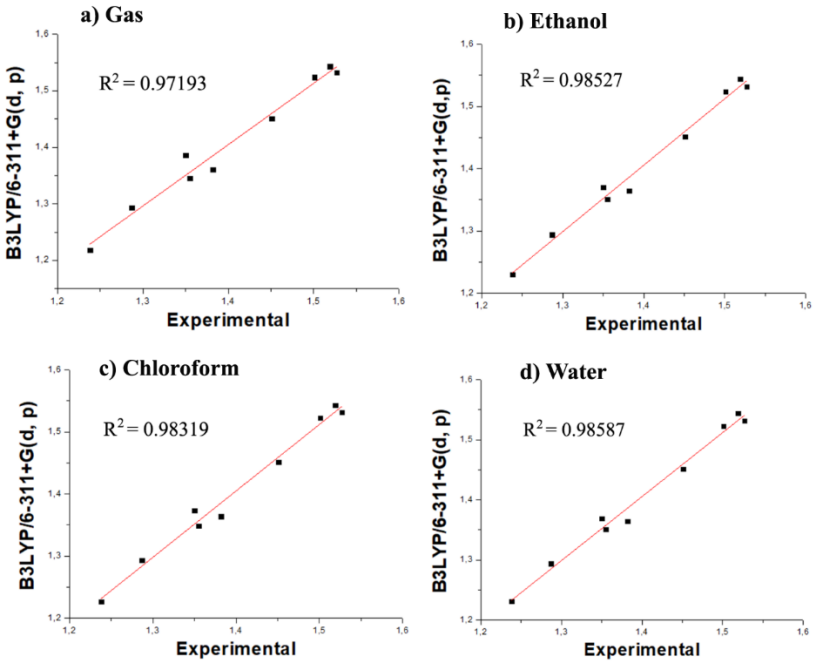


**Figure 3.2a** The regression analysis results of the bond lengths of the optimized molecular structure

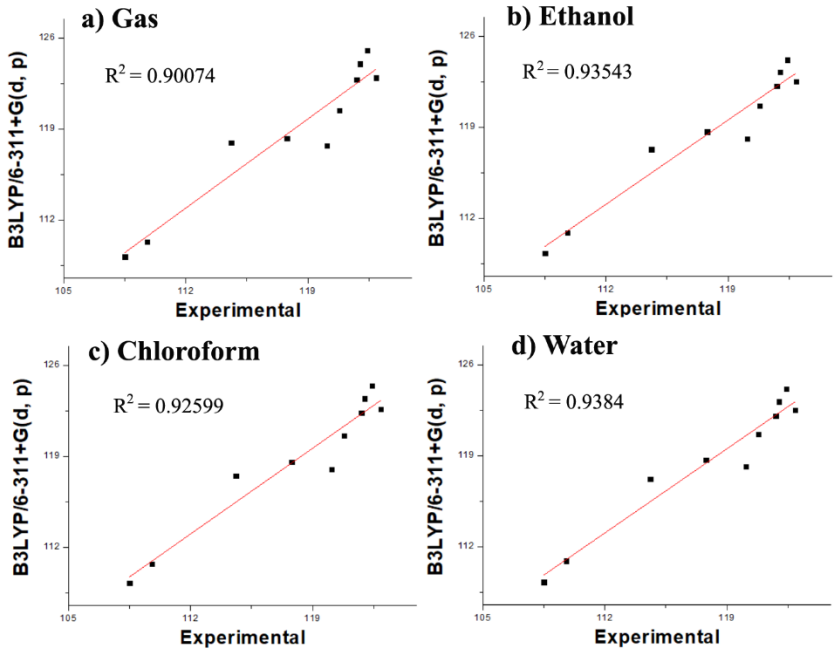


**Figure 3.2b.** The regression analysis results of the bond angles of the optimized molecular structure.

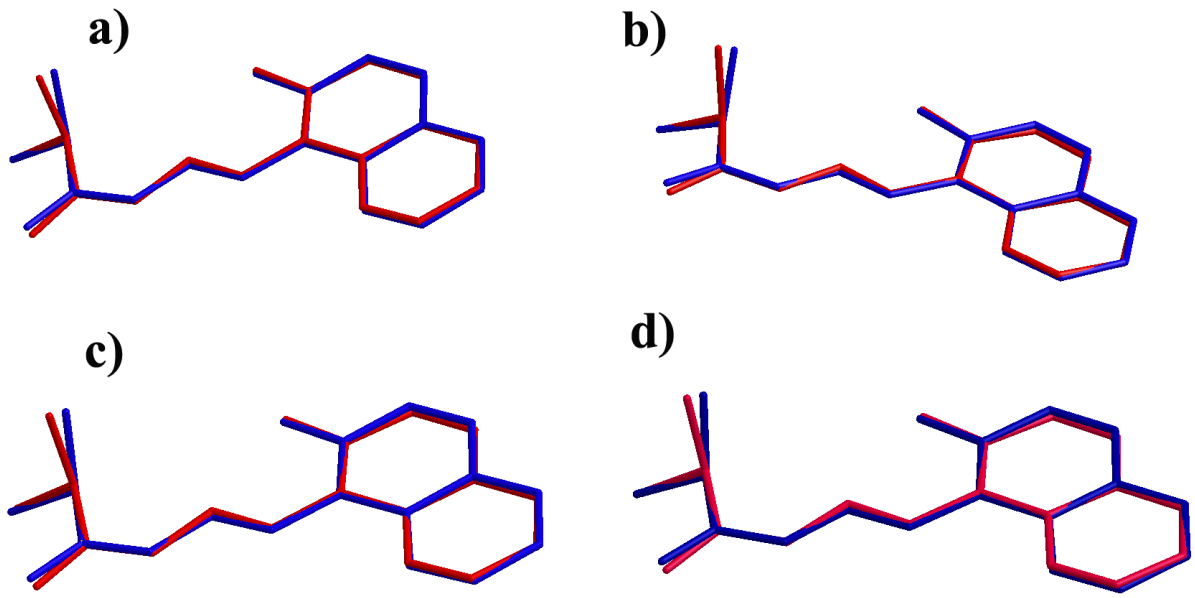


**Figure 3.3** Superpositions between the experimental results and the theoretical results, a) X-ray-B3LYP/6-311+G(d, p) Gas, b) X-ray-B B3LYP/6-311+G(d, p) Ethanol, c) X-ray-B3LYP/6-311+G(d, p) Chloroform, d) X-ray-B3LYP/6-311+G(d, p) Water

### 3.2 Molecular Electrostatics Potential (MEP) Surface Analysis of Molecular Structure

The molecular electrostatic potential (MEP) map of the molecular structure $C_{15}H_{16}N_2O_2$ was obtained by calculating the zero point energy in the water environment using the B3LYP/6-311+G(d, p) method in the ground state. The MEP map of a molecule is also important to explain the existence of intermolecular hydrogen bonds. The MEP map of a neutral molecule consists of different colors. Red represents the electron-rich nucleophilic region, blue represents the electron-poor electrophilic region, and gray represents the less positive region. Figure 3.4 shows the MEP map obtained from the water environment for the molecular structure. As seen in Figure 3.4, the oxygen atom of the isobutyric acid and the oxygen atom of the naphthol group of the molecular structure showed nucleophilic properties, while the nitrogen atom of the hydrazone group showed electrophilic properties. Single crystal X-ray diffraction analysis results of the molecular structure showed the presence of intermolecular hydrogen bonds such as O-H...N, N-H...O and C-H...N [2]. The MEP map obtained from the water environment supports the results by showing the presence of positive and negative potentials in the regions where these atoms are located.

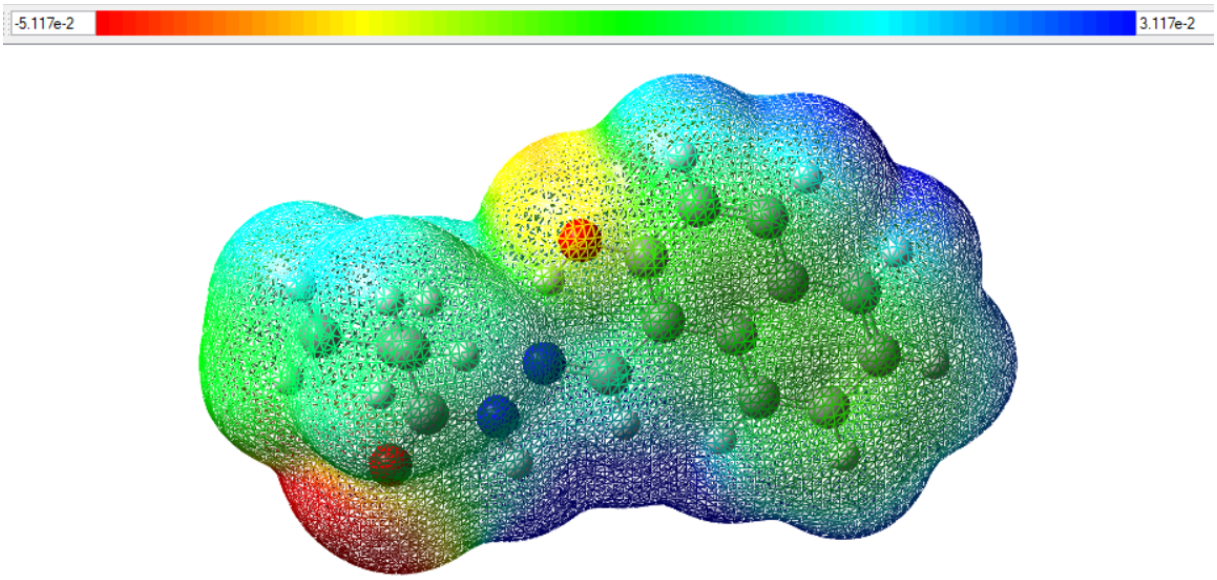


**Figure 3.4** Molecular electrostatic potential map of the compound $C_{15}H_{16}N_2O_2$ in water media by DFT method

### 3.3 Electronic properties of the molecular structure $C_{15}H_{16}N_2O_2$

Molecular orbital energy values, total energy and dipole moment of the $C_{15}H_{16}N_2O_2$ compound were calculated using the B3LYP/6-311+G(d, p) method in the ground state, both in gas and different solvent environments. The highest molecular orbital HOMO, which is occupied by electrons from molecular orbitals consisting of a linear combination of atomic orbitals, and the lowest molecular orbital LUMO, which is not occupied by electrons, are very important energy levels for understanding the chemical activity of a molecule [9-12]. These molecular orbitals are called frontier molecular orbitals. The narrower the HOMO-LUMO energy gap of a molecule, the softer and more unstable the molecular structure, but the wider the HOMO-LUMO gap, the harder and more stable the molecular structure and these soft molecules are chemically reactive and unstable [13, 14]. Donor electrons at the HOMO level of a molecule can be transferred to the acceptor LUMO level of metal ions when they receive sufficient energy. The HOMO-LUMO gap and the total energy of a molecule are stability indices of the molecule. A molecular structure with a narrow HOMO-LUMO gap and a high total energy is unstable and can easily transfer electrons. If a molecular structure has a wide HOMO-LUMO gap and a low total energy, that molecular structure is stable. In addition to this, the lower the value of chemical potential (μ), chemical hardness (η) and global electrophilicity index (ω) from the global reactivity parameters of the molecular structure, the better the donor properties will be [15, 16]. In Table 3.2, the calculated molecular orbital energy values, dipole moments and energy ranges for the molecular structure are given.

According to the calculation results, the total energy of the molecular structure obtained in the water environment is the lowest and the energy range is the widest.

**Table 3.2** The calculated frontier orbital energies, the total energies and HOMO-LUMO energy gaps (ΔE) of the molecular structure $C_{15}H_{16}N_2O_2$ by DFT method

| B3LYP | $E_{HOMO}$ (eV) | $E_{LUMO}$ (eV) | μ (D) | Total Energy (a.u.) | ΔE (eV) |
|---|---|---|---|---|---|
| 6-311+G (d, p) Gas | -5.9792 | -2.1595 | 3.2259 | -841.41916 | 3.8197 |
| 6-311+G (d, p) Chloroform | -5.9068 | -2.0719 | 4.5766 | -841.43544 | 3.8349 |
| 6-311+G (d, p) Ethanol | -5.8894 | -2.0504 | 5.0813 | -841.44227 | 3.8390 |
| 6-311+G (d, p) Water | -5.8812 | -2.0395 | 5.1967 | -841.44426 | 3.8417 |

Global reactivity parameters were obtained by using molecular orbital energy values of $C_{15}H_{16}N_2O_2$ compound. Ionization potential ($IP = -E_{HOMO}$) is the minimum energy required to remove an electron from the molecule. Electron affinity ($EA = -E_{LUMO}$) is defined as the amount of energy that increases when an electron is added to the molecule. Electronegativity ($\chi = (IP + EA)/2$) refers to the power of an atom in the molecule to attract electrons. The chemical potential ($\mu = -\chi$) is equal to the negative value of the electronegativity. Chemical hardness ($\eta = (IP - EA)/2$) is a measure of inhibition of charge transfer within the molecule. Molecules with high chemical hardness values have little or no intracellular charge. Chemical softness, is $S = 1/2\eta$ and electrophilicity index is $\omega = \mu^2/2\eta$ [1]. The global reactivity parameters obtained for the molecular structure are given in Table 3.3. As can be seen from Table 3.3, the hardest chemical structure was obtained from the water environment according to the global reactivity parameters, and it supports the most stable state of the structure.

Percent contribution to molecular orbital energies, transition wavelengths and UV-spectra of $C_{15}H_{16}N_2O_2$ compound in the excited state, both in gas and different solvent environments, were calculated using the Time Dependent Density Functional Theory (TD-DFT).

It was observed that the highest transition probability was 83% from the HOMO energy level to the LUMO level.

**Table 3.3** The calculated the energy values and global reactivity parameters of $C_{15}H_{16}N_2O_2$ the compound

| | 6-311+G (d, p) Gas | 6-311+G (d, p) Chloroform | 6-311+G (d, p) Ethanol | 6-311+G (d, p) Water |
|---|---|---|---|---|
| **IP (eV)** | 5.9792 | 5.9068 | 5.8894 | 5.8812 |
| **EA (eV)** | 2.1595 | 2.0719 | 2.0504 | 2.0395 |
| **χ (eV)** | 4.0693 | 3.9893 | 3.9699 | 3.9603 |
| **μ (eV)** | -4.0693 | -3.9893 | -3.9699 | -3.9603 |
| **η (eV)** | 1.9098 | 1.9174 | 1.9195 | 1.9208 |
| **S (eV)** | 0.2618 | 0.2608 | 0.2605 | 0.2603 |
| **ω (eV)** | 4.3352 | 4.1505 | 4.1055 | 4.0825 |

In Figure 3.5, the percentage contributions of functional groups in molecular structure from atomic orbitals to molecular orbitals are calculated. Atomic contributions for both HOMO and LUMO energy levels were higher than for naphthol group. The calculated UV-spectra is given in Figure 3.6.

### 3.4 Metal (Acceptor)-Ligand (Donor) Interaction

The metal-ligand bond strength between the interaction of acceptor and donor has recently been evaluated with the help of quantum chemical parameters, such as the energy lowering ΔE and charge transfer ΔN values [14, 17, 18]. The strength of the compound $C_{15}H_{16}N_2O_2$ as donor against an acceptor halides of Zn(II), Cd(II), Hg(II), Sn(II) and Sn(IV) was investigated using energy lowering ($\Delta E = -(\chi_A - \chi_B)^2 / 4 (\eta_A + \eta_B)$) and the charge transfer ($\Delta N = (\chi_A - \chi_B)/2 (\eta_A + \eta_B)$) parameters [17, 18]. The values of chemical potential (μ), chemical hardness (η) and electronegativity (χ) of metal halides, and values of energy lowering (ΔE) and the charge transfer (ΔN) are shown in Table 3.4.

**Table 3.3** The calculated absorption wavelength (λ) from 20 states, excitation energies (E), oscillator strength (f) and frontier orbital energies of the compound $C_{15}H_{16}N_2O_2$ by the TD-DFT method (HOMO: H ve LUMO: L).

| TD-DFT | Wavelengths (nm) | f | MO→MO (% Distributions) |
|---|---|---|---|
| 6-311+G(d, p) | 359 | 0.450 | H→L (83%) |
| Water | 308 | 0.091 | H-1→L (76%) |

| | | | |
|---|---|---|---|
| | 270 | 0.201 | H-2→L (75%) |
| | 258 | 0.416 | H→L+2 (46%) |
| | 232 | 0.488 | H-1→L+1 (41%) |
| | 207 | 0.287 | H-2→L+1 (35%) |
| 6-311+G(d, p) | 359 | 0.454 | H→L (83%) |
| Ethanol | 309 | 0.093 | H-1→L (76%) |
| | 270 | 0.200 | H-2→L (75%) |
| | 258 | 0.415 | H→L+2 (46%) |
| | 232 | 0.488 | H-1→L+1 (41%) |
| | 207 | 0.287 | H-2→L+1 (35%) |
| 6-311+G(d, p) | 361 | 0.467 | H→L (83%) |
| Chloroform | 309 | 0.103 | H-1→L (77%) |
| | 270 | 0.192 | H-2→L (76%) |
| | 259 | 0.422 | H→L+2 (47%) |
| | 234 | 0.479 | H-1→L+1 (38%) |
| | 208 | 0.245 | H-2→L+1 (32%) |
| 6-311+G(d, p) | 354 | 0.351 | H→L (80%) |
| Gas | 308 | 0.077 | H-1→L (74%) |
| | 268 | 0.120 | H-2→L (64%) |
| | 257 | 0.338 | H→L+2 (34%) |
| | 231 | 0.322 | H-1→L+1 (49%) |
| | 206 | 0.218 | H-2→L+8 (21%) |

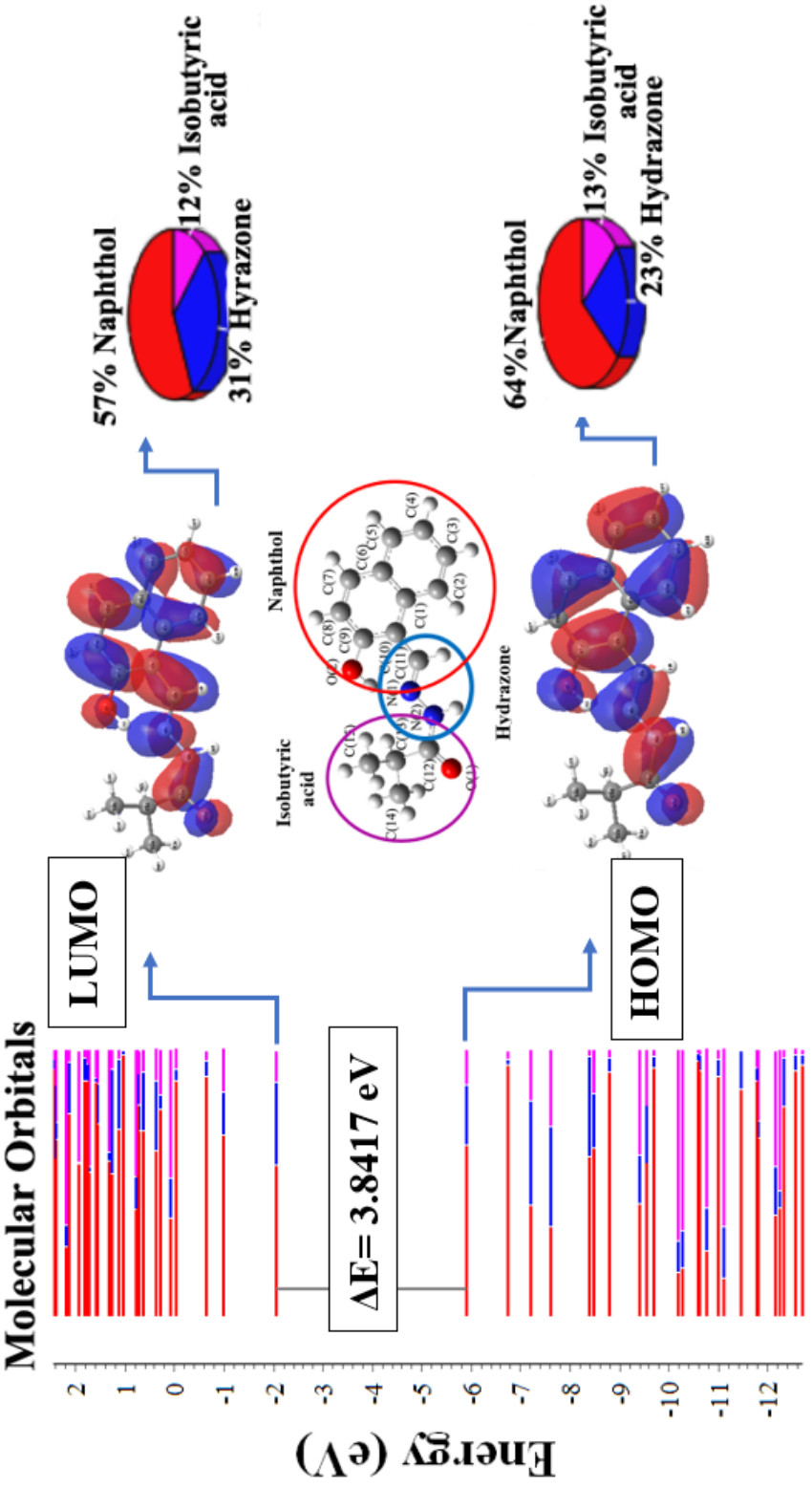


**Figure 3.5** The molecular orbital energies and percent distributions of the functional groups of the molecular structure in the water media by using B3LYP/6-311+G(d, p)

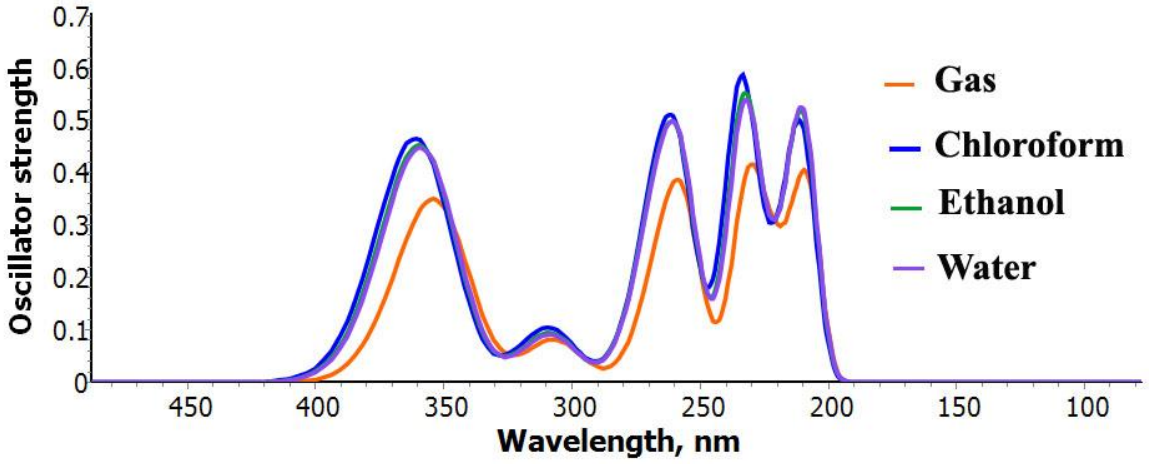


**Figure 3.6** The calculated UV-spectra of the compound $C_{15}H_{16}N_2O_2$ by TD-DFT/6-311+G(d, p)

**Table 3.4** Interaction of donor ($C_{15}H_{16}N_2O_2$) with acceptor halides ($MX_2$ and $MX_4$ (M = Zn, Cd, Hg, and Sn; X = Cl, Br, I)

| Acceptor | $\mu_A$ | $\eta_A$ | $\eta_D$ | $\chi_A$ | $\chi_D$ | $\Delta N$ | $\Delta E$ |
|---|---|---|---|---|---|---|---|
| $ZnCl_2$ | -4.4977716 | 3.087677 | 1.9208 | 4.4977716 | 3.9603 | 0.053651 | -0.01442 |
| $ZnBr_2$ | -4.4350494 | 2.783046 | 1.9208 | 4.4350494 | 3.9603 | 0.050458 | -0.01198 |
| $ZnI_2$ | -4.3345033 | 2.418821 | 1.9208 | 4.3345033 | 3.9603 | 0.043109 | -0.00806 |
| $CdCl_2$ | -4.2803526 | 2.958967 | 1.9208 | 4.2803526 | 3.9603 | 0.032789 | -0.00525 |
| $CdBr_2$ | -4.250284 | 2.697874 | 1.9208 | 4.250284 | 3.9603 | 0.031387 | -0.00455 |
| $CdI_2$ | -4.1344995 | 2.449842 | 1.9208 | 4.1344995 | 3.9603 | 0.019923 | -0.00173 |
| $HgCl_2$ | -4.4726011 | 2.733249 | 1.9208 | 4.4726011 | 3.9603 | 0.055033 | -0.0141 |
| $HgBr_2$ | -4.4281105 | 2.522496 | 1.9208 | 4.4281105 | 3.9603 | 0.052636 | -0.01231 |
| $HgI_2$ | -4.3776333 | 2.152557 | 1.9208 | 4.3776333 | 3.9603 | 0.051221 | -0.01069 |
| $SnCl_2$ | -5.4422792 | 2.338819 | 1.9208 | 5.4422792 | 3.9603 | 0.173949 | -0.12889 |
| $SnBr_2$ | -5.3560191 | 2.10589 | 1.9208 | 5.3560191 | 3.9603 | 0.1733 | -0.12094 |
| $SnI_2$ | -5.1875805 | 1.853096 | 1.9208 | 5.1875805 | 3.9603 | 0.162593 | -0.09977 |
| $SnCl_4$ | -6.9534641 | 2.459774 | 1.9208 | 6.9534641 | 3.9603 | 0.341631 | -0.51127 |
| $SnBr_4$ | -6.5586267 | 1.977316 | 1.9208 | 6.5586267 | 3.9603 | 0.333269 | -0.43296 |

| | | | | | | | |
|---|---|---|---|---|---|---|---|
| $SnI_4$ | -6.0964412 | 1.600574 | 1.9208 | 6.0964412 | 3.9603 | 0.3033 | -0.32394 |

The lower the value of chemical potential (μ) better will be the acceptor property. According to Table 3.4, it can be said that $SnCl_4$, $SnBr_4$, and $SnI_4$ have almost similar chemical potential value that is equal to about 6-7 eV. These results indicate that the acidic strength of $SnX_4$ (X = Cl, Br, I) is higher than $SnX_2$, and the $MX_2$ (M = Zn, Cd, Hg; X = Cl, Br, I) halides are weaker acceptors than Sn(II) and Sn(IV) halides.

The acceptor strength can be arranged in the following order:

$SnCl_4 \approx SnBr_4 \approx SnI_4 > SnCl_2 \approx SnBr_2 \approx SnI_2 > ZnCl_2 \approx ZnBr_2 \approx ZnI_2 \approx CdCl_2 \approx CdBr_2 \approx CdI_2 \approx HgCl_2 \approx HgBr_2 \approx HgI_2$

The metal bond strength between the interaction of acceptor (halides of Zn, Cd, Hg, and Sn) and donor ($C_{15}H_{16}N_2O_2$) increases as the energy lowering (ΔE) decreases and the charge transfer (ΔN) increases [14, 17, 18]. Where the acceptor is $MX_2$ (M = Zn, Cd, Hg, Sn; X = Cl, Br, I), the most stable complexes are formed by iodide halogen as the value of ΔE is lowest and the value of ΔN is highest.

According to values of ΔE, the sequence of stability of complexes formed by halogens of Zn(II), Cd(II), Hg(II) and Sn(II) are below.

$CdI_2 < CdBr_2 < CdCl_2 < ZnI_2 < HgI_2 < ZnBr_2 < HgBr_2 < HgCl_2 < ZnCl_2 < SnI_2 < SnBr_2 < SnCl_2$

The sequence of stability according to values of ΔN is very similar to this sequence. The acceptor strength of $SnX_4$ halides (X = Cl, Br, I) is in the following order:

$SnI_4 < SnBr_4 < SnCl_4$

Among all heavy metal halides, the most stable complex is formed with $C_{15}H_{16}N_2O_2$ and $SnCl_4$ (ΔE = -0.51127eV and ΔN = 0.341631 eV), and the least stable complex is formed with $C_{15}H_{16}N_2O_2$ and $CdI_2$ (ΔE = -0.00173 eV and ΔN = 0.019923 eV).

## 4. Conclusion

The molecular structure $C_{15}H_{16}N_2O_2$ was optimized by the DFT/B3LYP/6-311+G(d, p) method in the ground state in both gas and solvent environments with different polarization, and it was found that the bond parameters of the structure were more compatible with the experimental results in the literature in the water environment. By using the optimized molecular structures, a single point energy calculation was made in the ground state and MEP was obtained. According to the MEP map, it was observed that atoms in the nucleophilic and electrophilic regions of the molecule contributed to the intermolecular hydrogen bonds, which were explained according to the X-ray results. According to the single point energy calculation in the ground state, the molecular structure was found to be the most stable in the water environment. At the same time, it has emerged from the calculations that the highest contribution to the

HOMO and LUMO energy levels is from the naphthalene group of the molecular structure at 64% and 57%, respectively. Using TD-DFT, the molecular structure was found to have an absorption wavelength between 361-206 nm. By using the global reactivity parameters of the molecular structure, it was obtained that the molecular structure $C_{15}H_{16}N_2O_2$ made the most stable metal complex structure with $SnCl_4$ and the least stable structure with $CdI_2$ according to $\Delta N$ and $\Delta E$ values.

## Ethics in Publishing

There are no ethical issues regarding the publication of this study

## Acknowledgements

The authors are grateful to Asst. Prof. Dr. Ayşin ZÜLFİKAROĞLU from Amasya University for giving an idea to this study.

## References

[1] Zülfikaroğlu, A., Yüksektepe Ataol, Ç., (2020) Synthesis, Crystal Structure and Dft Studies of (E)-N'-(3,4-Dihydroxybenzylidene)Isobutyrohydrazide, Hydrazones Uses and Reactions, Isabella P. Østergaard(Ed.), Chapter 2(pp. 21-56). Nova Science Publishers. New York, ISBN: 978-1-53617-672-8. 21-56.

[2] Yüksektepe Ataol, Ç., Zülfikaroğlu, A., (2021) The Structure Analysis by DFT and X-ray Diffraction, LAMBERT Academic Publishing, Republic of Moldova Europe. ISBN: 978-613-5-84392-7. 1-57.

[3] Yang, Y. G., Hong, M., Xu, L. D., Cui, J. C., Chang, G. L., Li, D. C., Li, C. Z., (2016) Organotin(IV) complexes derived from Schiff base N1-[(1E)-(2-hydroxy-3-methoxyphenyl)methylidene]pyridine-3-carbohydrazone: Synthesis, in vitro cytotoxicities and DNA/BSA interaction, Journal of Organometallic Chemistry, 804 48–58.

[4] Moraes, R. S., Aderne, R. E., Cremona, M., Rey, N. A., (2016) Luminescent properties of a dihydrazone derived from the antituberculosis agent isoniazid: Potentiality as an emitting layer constituent for OLED fabrication, Optical Materials, 52 186–191.

[5] Tai, X. S., Wang, X., (2015) Synthesis and crystal structure of a 1D-chained coordination polymer constructed from $Ca^{2+}$ and 2-[(E)-(2-furoylhydrazono)methyl]benzenesulfonate, Crystals, 5 458–465.

[6] Andronie, L., Pop, I., Mireşan, V., Coroian, A., Raducu, C., Cocan, D., Coroian, C. O., (2014) Adsorption behavior of 1- and 2- Naphthol species on Ag colloidal nanoparticles, Human & Veterinary Medicine International Journal of the Bioflux Society, 6(4) 210-213.

[7] Frisch, M. J., Trucks, G. W., Schlegel, H. B., Scuseria, G. E., Robb, M. A., Cheeseman, J. R., Scalmani, G., Barone, V., Mennucci, B., Petersson, G. A., Nakatsuji, H., Caricato, M., Li,

X., Hratchian, H. P., Izmaylov, A. F., Bloino, J., Zheng, G., Sonnenberg, J. L., Hada, M., Ehara, M., Toyota, K., Fukuda, R., Hasegawa, J., Ishida, M., Nakajima, T., Honda, Y., Kitao, O., Nakai, H., Vreven, T., Montgomery, J. A., Peralta, Jr., J. E., Ogliaro, F., Bearpark, M., Heyd, J. J., Brothers, E., Kudin, K. N., Staroverov, V. N., Kobayashi, R., Normand, J., Raghavachari, K., Rendell, A., Burant, J. C., Iyengar, S. S., Tomasi, J., Cossi, M., Rega, N., Millam, J. M., Klene, M., Knox, J. E., Cross, J. B., Bakken, V., Adamo, C., Jaramillo, J., Gomperts, R., Stratmann, R. E., Yazyev, O., Austin, A. J., Cammi, R., Pomelli, C., Ochterski, J. W., Martin, R. L., Morokuma, K., Zakrzewski, V. G., Voth, G. A., Salvador, P., Dannenberg, J. J., Dapprich, S., Daniels, A. D., Farkas, O., Foresman, J. B., Ortiz, J. V., Cioslowski, J., Fox, D. J. (2009) Gaussian 09, Wallingford (CT, USA): Gaussian, Inc.

[8] Lee, C., Yang, W., Parr, R. G., (1988) Development of the Colle-Salvetti correlation-energy formula into a functional of the electron density Physical Review, B37 785-789.

[9] Kanmazalp, S. D., Başaran, E., Karaküçük-Iyidoğan, A., Oruç-Emre, E. E., Dege, N., (2017) X-ray structures and spectroscopic properties of chiral thiosemicarbazides as studied by computational calculations, Phosphorus, Sulfur, and Silicon and the Related Elements, 192(7) 856-865.

[10] Pekparlak, A., Tamer, O., Kanmazalp, S. D., Berber, N., Arslan, M., Avcı, D., Dege, N., Tarcan, E., Atalay, Y., (2018) Crystal structure, spectroscopic (FT-IR, 1H and 13C NMR) characterization and density functional theory calculations on Ethyl 2-(dichloromethyl)-4-methyl-1-phenyl-6-thioxo-1,6-dihydropyrimidine-5-carboxylate, Journal of Molecular Structure, 1171 762-770.

[11] Kanmazalp, S. D., Başaran, E., Karaküçük-Iyidoğan, A., Oruç-Emre, E. E., Sen, F., Dege, N., (2018) Synthesis, characterization, spectroscopy, X-ray structure and gaussian hybrid computational investigation of (−)-(S)-1-[2-(benzenesulfonamido)-3-phenylpropanoyl]-4-[(4-methyl)phenyl]thiosemicarbazide, Phosphorus, Sulfur, and Silicon and the Related Elements, 193(10) 675–684.

[12] Kanmazalp, S. D., Macit, M., Dege, N., (2019) Hirshfeld surface, crystal structure and spectroscopic characterization of (E)-4-(diethylamino)-2-((4-phenoxyphenylimino)methyl)phenol with DFT studies, Journal of Molecular Structure, 1179 181-191.

[13] Demircioğlu, Z., Albayrak Kaştaş, Ç., Büyükgüngör, O., (2015) Theoretical analysis (NBO, NPA, Mulliken Population Method) and molecular orbital studies (hardness, chemical potential, electrophilicity and Fukui function analysis) of (E)-2-((4-hydroxy-2-methylphenylimino)methyl)-3-methoxyphenol, Journal of Molecular Structure, 1091183-195.

[14] Zulfikaroglu, A., Bati, H., Dege, N., (2018) A theoretical and experimental study on isonitrosoacetophenone nicotinoyl hydrazone: Crystal structure, spectroscopic properties, NBO, NPA and NLMO analyses and the investigation of interaction with some transition metals, Journal of Molecular Structure, 1162 125-139.

[15] Zülfikaroglu, A., (2020a) The synthesis, experimental and theoretical characterization of a Pd(II) complex from diacetyl monoxime isobutyrohydrazone, Journal of Molecular Structure, 1209 127950.

[16] Zülfikaroglu, A., (2020b) DFT Computational Studies on Some Cobaloximes, Erzincan University Journal of Science and Technology, 13(3) 1299-1316.

[17] Boukli-Hacene, F., Merad, M., Ghalem, S., Soufi, W., (2014) DFT study of the interaction of Cu(II), Zn(II), Sn(II) with carbohydrates in aqueous solution, Journal of Chemistry and Chemical Engineering, 8 1009-1017.

[18] Singh, D., Ahmad, S., Singh, P. P., (2009) DFT based calculation of interaction energy between metal halides and organic bases, Journal of Molecular Structure: Theochem, 90 13-23.